



**HAL**  
open science

## **A new C-terminal hERG mutation A915fs+47X associated with symptomatic LQT2 and auditory-trigger syncope.**

Georges Christé, Olivier Thériault, Mohamed Chahine, Gilles Millat, Claire Rodriguez-Lafrasse, Robert Rousson, Isabelle Deschênes, Eckhard Ficker, Philippe Chevalier

### ► To cite this version:

Georges Christé, Olivier Thériault, Mohamed Chahine, Gilles Millat, Claire Rodriguez-Lafrasse, et al.. A new C-terminal hERG mutation A915fs+47X associated with symptomatic LQT2 and auditory-trigger syncope.: New LQT2-related hERG mutation A915fs+47X. Heart Rhythm, 2008, 5 (11), pp.1577-86. 10.1016/j.hrthm.2008.08.031 . inserm-00325603

**HAL Id: inserm-00325603**

**<https://inserm.hal.science/inserm-00325603>**

Submitted on 10 Oct 2008

**HAL** is a multi-disciplinary open access archive for the deposit and dissemination of scientific research documents, whether they are published or not. The documents may come from teaching and research institutions in France or abroad, or from public or private research centers.

L'archive ouverte pluridisciplinaire **HAL**, est destinée au dépôt et à la diffusion de documents scientifiques de niveau recherche, publiés ou non, émanant des établissements d'enseignement et de recherche français ou étrangers, des laboratoires publics ou privés.

## A new C-terminal hERG mutation A915fs+47X associated with symptomatic LQT2 and auditory-trigger syncope

Georges Christé, PhD,<sup>\*</sup> Olivier Thériault, MS,<sup>†</sup> Mohamed Chahine, PhD,<sup>†</sup> Gilles Millat, PhD,<sup>‖§</sup>, Claire Rodriguez-Lafrasse, PhD,<sup>‖§</sup> Robert Rousson, MD, PhD,<sup>‖</sup> Isabelle Deschênes<sup>¶</sup>, PhD, Eckhard Ficker, PhD<sup>¶</sup>, Philippe Chevalier, MD, PhD<sup>‡§</sup>

<sup>\*</sup> INSERM, ADR Lyon, Lyon, F-69003 France

<sup>†</sup> Le Centre de Recherche Université Laval Robert-Giffard and Department of Medicine, Laval University, Québec, Canada

<sup>‖</sup> Laboratoire de Cardiogénétique, Centre de Biologie Est, Hospices Civils de Lyon, Lyon, F-69003 France

<sup>‡</sup> Unité de Cardiologie et Soins Intensifs, Hôpital CardioVasculaire et Pneumologique L Pradel, Hospices Civils de Lyon, Lyon, F-69003 France

<sup>§</sup> Université de Lyon, Lyon, F-69003, France; Université Lyon 1, Lyon, F-69003, France

<sup>¶</sup> MetroHealth Medical Center, Cleveland, Ohio 44109, USA

Short title: New LQT2-related hERG mutation A915fs+47X

\* Address reprint requests and correspondence: Dr Georges Christé, Université Lyon 1 – Claude Bernard, Bâtiment Raphaël Dubois, 2<sup>o</sup> étage, 43 Bld du 11 Novembre 1918, F-69622 Villeurbanne Cedex, France. E-mail address: [christe@lyon.inserm.fr](mailto:christe@lyon.inserm.fr)

Tel: (33)4 78 40 00 57 Fax: (33)4 72 44 79 37 30

## **Abstract**

**Background:** A novel mutation of hERG (A915fs+47X) was discovered in a 32 year-old woman with torsades de pointes, long QTc interval (515 ms) and syncope upon auditory trigger. **Objective:** We explored whether the properties of this mutation could explain the pathology. **Methods:** Western blots and sedimentation analysis of del/WT hERG were used to analyze protein expression, assembly and trafficking. Whole-cell A915fs+47X (*del*) and wild-type (*WT*) currents were recorded in transiently transfected COS7 cells or *Xenopus* oocytes. **Results:** The tail current density at -40 mV after a 2 s depolarisation to +40 mV in COS7 cells expressing *del* was 36% of that for *WT*. Inactivation was 1.9-fold to 2.8-fold faster in *del* versus *WT* between -60 and +60 mV. In the range -60 to -10 mV, we found that a non-deactivating fraction of current was increased in *del* at the expense of a rapidly deactivating fraction, with a slowly deactivating fraction being unchanged. In *Xenopus* oocytes, expression of *del* alone produced 38% of *WT* currents whereas co-expression of 1/2 *WT* + 1/2 *del* produced 49.8%. Furthermore, the expression of *del* protein at the cell surface was reduced by about 50%. This suggests that a partial trafficking defect of *del* contributes to the reduction in *del* current densities and to the dominant negative effect when co-expressed with *WT*. In model simulations the mutation causes a 10% prolongation of action potential duration. **Conclusions:** Decreased current levels due to a trafficking defect may explain the long QT syndrome observed in our patient.

## **Keywords**

Long QT syndrome; Congenital defects; K-channel; Sudden death; Ventricular arrhythmias; human ether-à-go-go

## **Introduction**

The long QT syndrome results from mutations that are classified in ten classes (LQT1 to LQT10) according to the 10 different genes in which mutations have been identified<sup>1,2</sup>. LQT2 is the second most common variant of LQTS and accounts for 35%-40% of all mutations. It is related to mutations of the hERG (KCNH2) gene that cause a reduction of the rapid delayed rectifier current,  $I_{Kr}$ , a major determinant of ventricular action potential repolarization. This predisposes to arrhythmias causing syncope and occasionally sudden death. There is a strong link of auditory trigger for syncope in patients bearing a hERG mutation as compared to mutations in KCNQ1 (LQT1)<sup>3</sup>.

Many studies have contributed to our understanding of the molecular mechanisms involved in hERG channel dysfunction. Functional characterization of each mutation is important since it may help design therapeutic approaches adapted to the patient's mutational context<sup>4,5,6</sup>. In this work, we explore whether the electrophysiological properties of a novel C-terminal truncation mutation of hERG, found in a French family from Lyon, may account for the clinical phenotype and compare its properties with those of other C-terminal mutations.

## **Methods**

### *Engineering of plasmid cDNA*

*hERG* cDNA in pcDNA3 expression vector (kindly provided by G. Robertson) was co-transfected with the surface marker protein CD8 expression vector (EBO-pcD-CD8). The mutation hERG/del-2742-2775 was introduced into a pcDNA3 vector using a QuickChange<sup>TM</sup> site-directed mutagenesis kit according to the manufacturer's instructions (Stratagene, La Jolla, CA, USA), using the following nucleotide mutagenic sense and antisense primers:

hERG-del-2742-2775/F (cggccttggggccgggcccgggcccgtggggggagagcccgtccagtg) and hERG-del-2742-2775/R (cactggacgggctctccccccacggcccggcccggcccggcccgaagccg).

*Expression and electrophysiological studies in COS7 cells and Xenopus Oocytes*

The investigation conforms to the Guide for the Care and Use of Laboratory Animals published by the US National Institutes of Health (NIH Publication No. 85-23, revised 1996).

COS7 cells were plated at 30,000 cells per 35 mm diameter Petri dish in 1.5 ml DMEM. On the next day, every culture dish received 1  $\mu$ g of either hERG/WT (*WT*) or hERG/A915fs+47X (*del*) plasmid, together with 0.05  $\mu$ g of CD8 plasmid mixed with 3  $\mu$ l FuGENE 6 (ROCHE Diagnostics Corp.) in 100  $\mu$ l DMEM without serum. As a control named *NoH*, some dishes were processed identically but plasmids were omitted. Cells were incubated at 37°C (5% CO<sub>2</sub> in air) for 2 days before electrophysiological measurements.

A patch clamp amplifier (BioLogic RK400, Biologic, Meylan, France) was connected through a Labmaster 100 (Axon Instruments) AD/DA board, to a 486-SX based PC computer under Windows v3.11. Voltage-clamp was controlled by the CLAMPEX software of the pCLAMP package (version 4.0, Axon Instruments). Patch pipettes were pulled to an initial resistance of 0.5 to 1 M $\Omega$  when filled with intracellular solution containing (mM): 150 KCl; 2 MgCl<sub>2</sub>; 5 EGTA, 10 HEPES (pH=7.2, adjusted with KOH). Cells were exposed to anti-CD8-coated beads for 5 min (Dynabeads M-450 CD8, Dynal, Oslo, Norway) and washed twice with the bath solution to eliminate the unbound beads. Only cells decorated with beads were used for electrophysiological measurements, done at room temperature (20 to 22°C). Cells were superfused with an external solution containing (mM): 145 NaCl; 5 KCl; 2 MgCl<sub>2</sub>; 1 CaCl<sub>2</sub>; 10 HEPES (pH 7.4, adjusted with NaOH). The pipette junction voltage was estimated to 4.2 mV (JPCalc software, Peter H. Barry) and was not corrected for in the analyses. Cell capacitance ( $C_m$ ) was estimated <sup>7</sup> by fitting a single exponential function to the average of 20

hyperpolarizing pulses (10 mV) from -80 mV. Current densities (in pA/pF) were computed as the ratio of current to  $C_m$  for each cell.

The preparation of *Xenopus* oocytes was done as previously described<sup>8</sup>. Briefly, oocytes were subjected to collagenase treatment 2 mg/ml during 2.5-3 hours, stage V or VI oocytes were microinjected with 5 ng capped mRNA encoding either wild type (*WT*), mutant hERG or both. The oocytes were maintained at 18°C in a 2-fold diluted solution of Leibovitz's L-15 medium (Gibco, Grand Island, N.Y., USA) enriched with 15 mM 4-(2-hydroxyethyl)-1-piperazine-methanesulfonic acid (HEPES, pH 7.6, adjusted with NaOH), 1 mM glutamine, and 50 µg/µl gentamycin. Oocytes were used for experiments 1-3 days after injection.

The macroscopic potassium currents from the mRNA-microinjected oocytes were recorded using voltage-clamp technique with two 3M KCl-filled microelectrodes. Membrane potential was controlled by a Warner oocyte clamp (Warner Instrument Corp., Hamden, CT). Voltage commands were generated by computer using pCLAMP software version 5.5 (Axon Instruments, Inc., Foster City, CA). Currents were filtered at 2 kHz (-3 dB; 4 pole Bessel filter). Solutions: The Ringer's bathing solution contained (mM): 116 NaCl, 2 KCl, 0.9 CaCl<sub>2</sub>, 2.9 MgCl<sub>2</sub>, 5 HEPES; pH was adjusted to 7.6 at 22°C with NaOH. Ringer solution was low in Ca<sup>2+</sup> to reduce the contribution of Ca<sup>2+</sup> activated chloride currents. All experiments were carried out at room temperature (22°C).

Only experiments pertaining to the coexpression of *WT* and *del* hERG were conducted in *Xenopus* oocytes (Panel E of figure 4). All other electrophysiological experiments were carried out in COS7 cells.

#### *Western blot analysis.*

The polyclonal anti-hERG antibody (rabbit hERGbasic) used in the present study was raised in rabbits against a C-terminal peptide corresponding to hERG aa residues 883-901 as

previously described<sup>9</sup>. hERGBasic antiserum was purified on an affinity column consisting of the C-terminal peptide used for immunization (aa 883-901: RQRKRKLSFRRRTDKDTEQ). HEK293 cells were transfected with either the *WT* or *del* plasmid using Fugene 6. Two days later, they were solubilized for 1 h at 4 °C in lysis buffer containing 150 mM NaCl, 1 mM EDTA, 50 mM Tris, pH 8.0, 1% Triton X-100 and protease inhibitors (Complete, Roche Diagnostics, Indianapolis, IN). Protein concentrations were determined by the BCA method (Pierce, Rockford, IL). Proteins were separated on SDS polyacrylamide gels, transferred to polyvinylidene difluoride membranes and developed using hERGBasic antibody followed by ECL Plus (GE Healthcare, Piscataway, NJ).

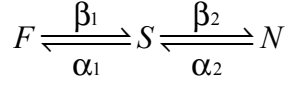
#### *Sucrose gradients*

HEK293 cells expressing *WT* or *del* hERG were lysed in Digitonin lysis buffer containing 150 mM NaCl, 10 mM Tris, pH 7.4, 1% digitonin and protease inhibitors (Complete, Roche Diagnostics, Indianapolis, IN). Soluble material (400-800 µg total protein) was layered onto 15-45% sucrose gradients (150 mM NaCl, 10 mM Tris, pH 7.4, 0.1% digitonin). Gradients were made using BIOCAMP Model 117 Gradient Mate (BIOCAMP, Fredericton, NB, Canada) according to the operator's manual, and centrifuged in a Beckman SW50.1 rotor at 48000 rpm for 16-18hr at 4°C, with brakes fully applied. After centrifugation, 275 µl fractions were collected manually from the top of gradients. Aliquots of individual fractions (150 µl) were concentrated using PAGEprep Protein Clean-Up and Enrichment Kit (Pierce) prior to loading onto a SDS/PAGE gel for Western blotting.

#### *Computer modelling*

A model of guinea-pig ventricular myocyte<sup>10</sup> was used, in which the original  $I_{Kr}$  formulation<sup>11</sup> was modified.

The  $I_{Kr}$  model was modified to include three subpopulations of channels with different deactivation kinetics. Channels moved from one subpopulation to the other in a sequential manner:



( $F$ : fastly deactivating;  $S$ : slowly deactivating;  $N$ : non-deactivating).

The rate constants of interconversion,  $\alpha_1$ ,  $\beta_1$ ,  $\alpha_2$  and  $\beta_2$  were functions of voltage of the shape:  $\alpha = u + v * \exp[(V_m - V_h)/s]$  where  $u$ ,  $v$ ,  $V_h$  and  $s$  are constants and  $V_m$  is the membrane voltage.

The voltage-dependent steady-state values of the fraction of channels in each subpopulation are resolved using:

$$F_\infty = 1/(1 + k_1 + k_1 * k_2); \quad N_\infty = k_1 * k_2 / (1 + k_1 + k_1 * k_2); \quad S_\infty = 1 - F_\infty - N_\infty;$$

with  $k_1 = \beta_1/\alpha_1$  and  $k_2 = \beta_2/\alpha_2$ .

The values of parameters  $u$ ,  $v$ ,  $V_h$  and  $s$  proper to each of the four rate constants were adjusted so that the steady-state values of the fractions versus voltage fitted experimental data. Transitions between the three populations were assumed instantaneous. All three subpopulations had the same properties of activation, inactivation and recovery from inactivation.

The second change to the  $I_{Kr}$  model was to reformulate the time-dependent changes in the inactivation variable ( $Y_r$ ) in order to allow the time constant of recovery from inactivation ( $\tau_{ri}$ ) to differ from that of inactivation ( $\tau_i$ ):

$$\text{if } (Y_{r\infty} - Y_r) < 0: \quad \frac{dY_r}{dt} = \frac{(Y_{r\infty} - Y_r)}{\tau_i}, \text{ otherwise: } \frac{dY_r}{dt} = \frac{(Y_{r\infty} - Y_r)}{\tau_{ri}},$$

where  $Y_{r\infty}$  is the steady-state inactivation variable.

In a similar way, the formulation of time-dependent changes in the activation variable ( $X_r$ ) was altered to allow for the time constant of deactivation ( $\tau_{da}$ ) to differ from that of activation ( $\tau_a$ ):

$$\text{if } (X_{r\infty} - X_r) > 0: \frac{dX_r}{dt} = \frac{(X_{r\infty} - X_r)}{\tau_a}, \text{ otherwise: } \frac{dX_r}{dt} = \frac{(X_{r\infty} - X_r)}{\tau_{da}},$$

where  $X_{r\infty}$  is the steady-state value of the activation variable. There was one such equation for each of the three deactivation subpopulations, for the non-deactivating subpopulation,  $dX_r/dt$  was set to 0 if  $(X_{r\infty} - X_r) \leq 0$ .

The steady-state inactivation and activation variables were described by Boltzmann functions of voltage, allowing them to remain unaltered whenever the time constants of inactivation or recovery from inactivation or of activation or deactivation were changed. The time constants of deactivation (separate for each subpopulation) and time constants of activation, inactivation and recovery from inactivation were functions of membrane voltage adjusted to reproduce our data.

The equation for the global  $I_{Kr}$  current was:

$$I_{Kr} = \bar{g}_{Kr} * \sqrt{\frac{[K^+]_e}{5.4}} * (V_m - E_{Kr}) * (A_F + A_S + A_N)$$

where  $A_F = X_{r_F}^3 * Y_r * F_\infty$ ,  $A_S = X_{r_S}^3 * Y_r * S_\infty$  and  $A_N = X_{r_N}^3 * Y_r * N_\infty$  are the respective fractions of channels open in each subpopulation,  $\bar{g}_{Kr}$  is the maximal conductance of the  $I_{Kr}$  current,  $[K^+]_e$  the extracellular  $K^+$  concentration,  $V_m$  the transmembrane voltage and  $E_{Kr}$  the reversal voltage of the  $I_{Kr}$  current. The activation variable was elevated to power 3 to account for the delayed onset of activation<sup>12</sup>.

With proper adjustment of parameters, this formulation satisfactorily reproduced the behaviour of *WT* or *del* hERG currents recorded in voltage-clamp at room temperature. To produce action potentials, each kinetic process was adjusted to 37°C by applying the specific voltage shifts and Q10 values defined for hERG channels<sup>13</sup>.

### *Data analysis and statistics*

Analysis of electrophysiological data was done using macros in CLAMPFIT (pCLAMP v6.0, Axon Instruments) and custom programs written under MATLAB (The MathWorks Inc.). Mathematical modelling was done in MATLAB. Statistical tests and final figures were done under Origin 4 (OriginLab Corp., Northampton, MA, USA). Results are expressed as mean  $\pm$  standard error of the mean (sem), the number of measurements (n) is indicated in parentheses. Unpaired Pearson's t-test was used and the p values are indicated in text and figures.

## **Results**

### *Clinical background*

The proband, a woman, began to experience syncopal events at the age of 18, typically when the telephone rang. At the age of 28, hypokalaemia favoured by self-provoked vomiting caused repeated episodes of torsades de pointes (figure 1A) which were treated with beta-blocker therapy. She presented with a QTc of 515 ms. During a follow-up of 7 years and a therapy with nadolol (40 mg per day) she remained asymptomatic.

### *Figure 1 near here*

Her brother and one of her two sons have a long QT interval without any symptoms (QTc of 475 and 480 msec, respectively). Her paternal aunt has had a history of unexplained syncope. Genetic analyses revealed the presence of a novel C-terminal mutation of hERG in these three members of the proband's family<sup>14</sup> (see the family pedigree in figure 1B).

### *Mutation structure*

In this 34 bp deletion of bases 2742 to 2775, the frameshift leaves aa residue G914 preserved. A premature stop codon occurs at position 2883 of the new base sequence. Thus, an extraneous 47 aa sequence is appended after G914 and replaces the last 245 C-terminal aa of *WT* hERG.

### *Figure 2 near here*

Consequently, *del* protein has a lower apparent molecular weight on Western blots than *WT* (figure 2A). While hERG *WT* is synthesized as a fully-glycosylated cell surface protein of about 160 kDa and a core-glycosylated ER resident form of about 135 kDa, the fully- and core-glycosylated forms of *del* protein are considerably smaller at about 120 and 100 kDa, respectively. Furthermore, quantitative analysis of 5 independent Western blot experiments (figure 2B) shows that in comparison to *WT*, less fully-glycosylated *del* protein is produced on transfection of equivalent amounts of cDNA. Since the deletion in hERG is thought to remove a putative assembly site, we analyzed *WT* and *del* assembly status by separating digitonin lysates on a 15-45% sucrose gradient. Figure 2C shows a Western blot analysis of *WT* and *del* gradient fractions. Both proteins are distributed in two major peaks with the majority present in the tetrameric peak formed by fractions 13-16. In *WT*, fractions 6-8 form a smaller yet distinct secondary peak which we equate with channel monomers and dimers. However in *del*, the relative protein content of fractions 5 to 9 is small, i. e.: *del* monomers/dimers appear to be shifted to larger molecular weights when compared to the corresponding *WT* forms as if under non-denaturing conditions the smaller *del* protein is present in complex with another, currently unknown protein.

Taken together, these data suggest that *del* channels assemble properly but yet exhibit a partial trafficking defect which is most likely responsible for the reduced whole cell current densities observed with *del* versus *WT* in electrophysiological experiments (see below).

*Properties of mutated channels hERG/A915fs+47X as compared to hERG/WT in COS7 cells*

**Current-voltage relations, voltage dependence of steady-state activation and activation time course**

Cells expressing hERG/A915fs+47X (*del*) had a cell capacitance ( $C_m$ ) similar to that of cells transfected with hERG/WT (*WT*) as reported in Table 1.

*Table 1 near here*

Typical current families generated in response to a two-pulse protocol by cells expressing *WT* or *del* are illustrated in panels A and B respectively, of figure 3.

*Figure 3 near here*

The current at the end of the prepulse (2 seconds) is characteristic for hERG with a clear apparent inward rectification (figure 4A). For each cell, the I/V relation of the tail current in pulse P2 ( $I_{\max P2}$ , figure 4B) was fitted with a Boltzmann function to evaluate the dependence of the steady-state activation variable on the prepulse voltage ( $V_{P1}$ )<sup>15</sup>. In figure 4C on the right, the normalized currents are superimposed with the fitting function, computed from the mean values of  $V_{ha}$  (the voltage for half activation) and of  $k_a$  (the slope factor) in Table 1. It appears that the voltage dependence of steady-state activation was not affected by the mutation.

*Figure 4 near here*

The average maximal current density at + 50 mV in pulse P2 (figure 3B and Table 1) was 2.76 fold lower in *del* than in *WT* cells.

The time constant of activation was evaluated as indicated in figure 4D<sup>12</sup>. The mutation did not cause any significant change in the activation time constant of the hERG current at voltages from -20 to +60 mV (figure 4D).

Panel E of figure 4 compares the amplitudes of peak tail currents at -40 mV in *Xenopus* oocytes co-injected with *WT* and *del* cDNAs with those of oocytes injected with either *WT* or *del* cDNA. The decrease in current related to the mutation confirms the finding in COS7 cells (see above). These results are further analysed in the discussion.

### **Voltage dependence of steady state inactivation**

A 3-pulse protocol was used: a maximally activating 2 sec pulse P1 to +50 mV was followed by a short (24 ms) pulse P2 to a variable voltage level ( $V_{P2}$ ). The amplitude of the current upon returning to +50 mV was normalized to its maximum for most negative  $V_{P2}$  values, after correction for the fast deactivation during P2<sup>16</sup>. The resulting data were fitted by a Boltzmann function characterized by the voltage for half inactivation ( $V_{hi}$ ) and the slope factor ( $k_i$ ). These were not significantly different between *del* and *WT* (see values in Table 1). Thus the steady-state inactivation versus voltage relation (see the plots in figure 4C, left traces) is not affected by the mutation.

### **Time course of inactivation, reversal voltage and maximal conductance**

A 3-pulse protocol was used. A 2 sec pulse P1 to +40 mV was followed by a 8 ms pulse P2 to -120 mV to relieve inactivation. The fast time constant of current decay in the test pulse (P3) to various voltages evaluated the inactivation time constant<sup>12</sup>. As shown in figure 5 the mutated channel (*del*) inactivates 1.9-fold to 2.8-fold faster than *WT* between -60 and +60 mV.

*Figure 5 near here*

Extrapolation of the fitted curve to time 0 of pulse P3 yielded the instantaneous current-voltage relation (not shown)<sup>12</sup>. Its intercept with the voltage axis evaluates the reversal voltage ( $E_{rev}$ ) of the hERG current (Table 1), which was almost identical in *del* and *WT*. Thus, the ionic selectivity of the channel is not changed by the mutation.

### **Time course of deactivation of the hERG current**

We recorded the current response during a 5.8 s test pulse at various voltages after a 2 s maximally activating prepulse to +40 mV (see inset to figure 6A). The current shows fast recovery from inactivation, followed by a slower, bi-exponential deactivation. The time constant of recovery from inactivation (figure 6B), was not affected by the mutation. The fast and slow exponential deactivation processes were estimated at all voltages by fitting a two-exponential function plus offset to the current traces from 80 ms to the end of the test pulse:

$$y = I_{fast} \cdot \exp(-t / \tau_{fast}) + I_{slow} \cdot \exp(-t / \tau_{slow}) + I_{infinity}$$

comprising a fast component with amplitude  $I_{fast}$  and time constant  $\tau_{fast}$ , a slow component with amplitude  $I_{slow}$  and time constant  $\tau_{slow}$ ,  $I_{infinity}$  being the amplitude of the component that did not deactivate. These parameters were iteratively adjusted using the "Simplex" method within MATLAB until the sum of squared differences with experimental data was minimal.

There was no significant difference at any voltage between *del* and *WT* currents in the fast deactivation time constant ( $\tau_{fast}$ ) or in the slow one ( $\tau_{slow}$ ) (figure 6C).

*Figure 6 near here*

### **Amplitudes of the components of current decay**

We also explored in each cell the voltage dependence of the initial amplitudes of the fast and slow deactivation components and that of the non-deactivating component. An example of this analysis is given in figure 6D where it appears that the sum of the amplitudes of the

three components (thick line) is the fully activated current-voltage relation. We further computed the ratio of each of these three components to the total current in order to evaluate the respective fraction of the current contributed by each of these three processes. The voltage dependence of these fractions is shown in figure 6, (panels E, F, G). It appears that the fast deactivating fraction was significantly lower for *del* current than for *WT* at all voltages from -70 to -10 mV. In contrast, the non-deactivating fraction was significantly higher in *del* than in *WT* in the same voltage range. The slowly deactivating fraction was slightly changed.

Although the different components of deactivation of *WT* hERG have been studied in the past<sup>17</sup>, a careful quantitative analysis of the relative contribution of fast-, slow- and non-deactivating fractions at various voltages has not been previously reported. We interpreted these changes as due to the distribution of hERG channels among three kinetically differently deactivating subsets (see Methods) and included this concept into a model of single ventricular myocyte to test the impact on AP configuration (see in Discussion).

## Discussion

To date, about 290 mutations have been found in the hERG gene and related to Romano-Ward Syndrome and Sudden Infant Death Syndrome. Of these mutations, 91 occur in the C-terminal region. The novel mutation found in this study is a frameshift/deletion at aa 915 in the C-terminal region of hERG that removes a putative assembly domain of the channel protein. Among 38 mutations distal to this site, 25 are deletions<sup>18</sup>. When co-expressed with *WT*, mutated hERG proteins may cause a reduction of hERG currents due to altered trafficking<sup>19,20</sup>, altered subunit assembly<sup>19</sup>, or by rendering heterotetramers dys- or hypo-functional<sup>16</sup>.

### *Reduced cell surface expression and current density*

Our Western analysis showed that only about half of *del* hERG attains the fully glycosylated mature state when compared to *WT* (figure 2A-B). It has been shown previously that the fully-glycosylated form of hERG is located at the cell surface<sup>21,22</sup>. Thus, the observed reduction in the fully-glycosylated protein form of *del* is mainly responsible for the lower membrane current densities observed in COS7 cells (36%; figure 4B and Table 1) as well as in *Xenopus* oocytes (37%; figure 4E). The phenotype of *del* was further evaluated upon co-expression with *WT*, to mimic the heterozygous state found in our patient. Co-injection of 2.5 ng *del* + 2.5 ng *WT* cDNA in *Xenopus* oocytes yielded peak tail current densities that represented about 48% of those recorded on injection of 5 ng *WT* cDNA. In contrast, injection of 5 ng *del* cDNA yielded 37% of the tail current densities observed with 5 ng *WT*. If *del* and *WT* were not be able to co-assemble and expressed currents independently, we would expect 68.5% (50% *WT* + 37/2% *del*) of *WT* currents assuming that the amount of hERG current generated per oocyte is proportional to the amount of cDNA injected<sup>23</sup>. Thus, co-expression decreased hERG current density when compared to independently expressing *del* and *WT* subunits, but increased current density when compared to *del* expressed in isolation. This complex behaviour is explained best with co-assembly of *del* and *WT* channel subunits into heterotetramers. Heterotetramer formation is not unlikely, since fractionation experiments of *del* on sucrose gradients have shown that the assembly of *del* subunits into tetramers was not compromised (fig 2C). Using a binomial formula<sup>24</sup>, and assuming that the presence of one or more *del* subunit in a tetramer reduces its trafficking to 50% (or to 37%), the overall current when ½ *WT* and ½ *del* are co-expressed is 53% (respectively 42%) of that with *WT* alone. The value of 48% found in our co-expression experiments agrees with this view. Taken together, our data suggest that *WT* and trafficking-deficient *del* subunits most

likely assemble into trafficking-deficient heterotetramers thereby producing a dominant negative effect.

The assembly of *del* into tetramers is somewhat unexpected, since the TCC (tetramerizing coiled-coil) domain - found within aa region 1018-1122<sup>19</sup> - is absent in hERG/A915fs+47X. Nevertheless, the sucrose gradient data clearly indicate that assembly is not affected in *del*, confirming that the TCC may not be an absolute requirement for proper tetramer formation<sup>19</sup>. At the same time, the deletion seems to produce a small shift on sucrose gradients in line with the formation of novel protein-protein interactions, possibly with components of the cellular quality control machinery, which may be ultimately responsible for the reduced surface expression of *del* or *del/WT* heterotetramers.

#### *Comparison with other C-terminal truncation mutations*

Another C-terminal truncation, R1014X, has also been associated with a trafficking defect in combination with a strong dominant negative effect exerted on *WT* hERG, while tetrameric assembly was not impaired<sup>19</sup>. Despite the fact that *del* (A915fs+47X) removes a much larger part of the C-terminus (245 aa) than R1014X (146 aa), the reduction in current density was less pronounced. Thus, functional effects of a particular deletion may not simply correlate with the extent of the deletion. In addition, *del* was also characterized by a 2-fold acceleration of current inactivation. Although a number of C-terminal mutations were found in LQT2 patients, only few have been characterized at the functional level<sup>18</sup>. For example, the deletion of up to 215 aa had no effects on biophysical properties, whereas deletion of either 236 or 278 aa accelerated current deactivation and speeded up recovery from inactivation<sup>25</sup>. In marked contrast, removal of 245 aa in *del* did not alter any of these parameters. Similarly, neither G965X nor R1014PfsX39 or V1038AfsX21, three other C-terminal deletions found in LQT2 patients, changed current kinetics, with only G965X decreasing current amplitudes (33% of

*WT* hERG)<sup>26</sup>. Finally, the two-fold acceleration of current inactivation in *del* is rather unique. Only one other C-terminal deletion/frameshift mutation has been described so far (hERG 1122fs/147) that accelerated current inactivation in a similar manner<sup>27</sup>. Interestingly, the replacement of the last 37 C-terminal aa by a 147 extraneous aa sequence was responsible for this phenomenon in hERG 1122fs/147<sup>27</sup>. Likewise, addition of an extraneous sequence of 47 aa in *del* may play a role in the altered biophysical properties of this channel. While these results suggest that the hERG C-terminus contributes to channel inactivation, a mechanistic explanation is currently not at hand.

#### *Proarrhythmic consequences of the mutation*

The three changes caused by the *del* mutation, -decreased current density, accelerated inactivation and modified pattern of deactivation kinetics-, were introduced in a computer model with a modified formulation of  $I_{Kr}$  (see Methods). This model was used to evaluate the effects of the mutation-induced changes on the ventricular action potential (AP).

#### *Figure 7 near here*

Starting from a control action potential (AP) elicited at 1 Hz (see bar 1 in figure 7A), wildtype  $I_{Kr}$  parameters were altered to reproduce various combinations of the effects observed for the *del* mutation (see the legend to figure 7). Introduction of accelerated inactivation (bar 2), of altered deactivation (bar 3), or of both altered inactivation and deactivation parameters (bar 4), slightly shortened the duration to 90% repolarization ( $APD_{90}$ ) of the following AP. In contrast, a two-fold decrease of the maximal conductance of  $I_{Kr}$  (bar 5) considerably lengthened  $APD_{90}$  as compared to *WT* (bar 1). When accelerated inactivation (bar 6) and altered deactivation (bar 7) were also added,  $APD_{90}$  was unchanged or slightly shortened versus decreased  $I_{Kr}$  conductance alone (bar 5). When all mutation-induced changes were introduced simultaneously, APD lengthening (bar 8 versus bar 1) was similar to what

was observed when only the  $I_{Kr}$  conductance was decreased (bar 5 versus bar 1). The accelerated inactivation caused by the mutation did not change the time course of the action potential since inactivation reaches its steady-state within 12 ms (3 x time constant of 4 ms at +30 mV), and within 5 ms when inactivation is accelerated 2.5-fold. Since steady-state inactivation is not altered by the mutation, the amount of current carried by hERG should only be decreased at very early time points of the AP when inward currents dominate. The change in current deactivation does also not influence AP duration because at voltages corresponding to the AP plateau, most channels are in the slow- and non-deactivating fractions, so that overall deactivation during an AP is negligible. Taken together, the most prominent effect of the mutation on AP duration is attributable to the decrease of  $I_{Kr}$  current amplitude which reflects mostly disrupted channel trafficking.

The effect of all the mutation-induced changes on the AP and the concomitant  $I_{Kr}$  current (figure 4B and 4C) is reflected in an AP prolongation of 9.6% when compared to *WT*. This could account for the LQT phenotype observed and would explain the increased susceptibility to triggers of early after-depolarisations involved in torsades de pointes and related syncope seen in our patient.

### *Conclusion*

This novel heterozygous A915fs+47X mutation alters several biophysical hERG channel properties and produces a pronounced trafficking defect which underlies its dominant negative behaviour. As a result,  $I_{Kr}$  currents are reduced by 50% which may explain the proarrhythmic events observed in our patient.

## **Acknowledgements**

This work was supported by a research grant to G. Christé from the Fédération des Maladies Orphelines, Paris. G. Christé is grateful to colleagues at the laboratory of "Physiologie Intégrative, Cellulaire et Moléculaire", UMR CNRS 5123, Université Lyon 1, who welcomed him for doing most of the present work. This study was also supported by grants from the Heart and Stroke Foundation of Québec (HSFQ) and the Canadian Institutes of Health Research (CIHR). M. Chahine is an Edwards Senior Investigator (Joseph C. Edwards Foundation).

## References

1. Lehnart SE, Ackerman MJ, Benson DW, Jr., Brugada R, Clancy CE, Donahue JK, George AL, Jr., Grant AO, Groft SC, January CT, Lathrop DA, Lederer WJ, Makielski JC, Mohler PJ, Moss A, Nerbonne JM, Olson TM, Przywara DA, Towbin JA, Wang LH, Marks AR: Inherited arrhythmias: a National Heart, Lung, and Blood Institute and Office of Rare Diseases workshop consensus report about the diagnosis, phenotyping, molecular mechanisms, and therapeutic approaches for primary cardiomyopathies of gene mutations affecting ion channel function. *Circulation* 2007; 116:2325-2345.
2. Saenen JB, Vrints CJ: Molecular aspects of the congenital and acquired Long QT Syndrome: clinical implications. *J Mol Cell Cardiol* 2008; doi:10.1016/j.yjmcc.2008.01.006:
3. Schwartz PJ, Priori SG, Spazzolini C, Moss AJ, Vincent GM, Napolitano C, Denjoy I, Guicheney P, Breithardt G, Keating MT, Towbin JA, Beggs AH, Brink P, Wilde AA, Toivonen L, Zareba W, Robinson JL, Timothy KW, Corfield V, Wattanasirichaigoon D, Corbett C, Haverkamp W, Schulze-Bahr E, Lehmann MH, Schwartz K, Coumel P, Bloise R: Genotype-phenotype correlation in the long-QT syndrome: gene-specific triggers for life-threatening arrhythmias. *Circulation* 2001; 103:89-95.
4. Moss AJ, Kass RS: Long QT syndrome: from channels to cardiac arrhythmias. *J Clin Invest* 2005; 115:2018-2024.
5. Kass RS, Moss AJ: Mutation-specific pharmacology of the long QT syndrome. *Handb Exp Pharmacol* 2006;287-304.
6. Napolitano C, Bloise R, Priori SG: Gene-specific therapy for inherited arrhythmogenic diseases. *Pharmacol Ther* 2006; 110:1-13.
7. Benitah JP, Gomez AM, Bailly P, Da Ponte JP, Berson G, Delgado C, Lorente P: Heterogeneity of the early outward current in ventricular cells isolated from normal and hypertrophied rat hearts. *J Physiol* 1993; 469:111-138.
8. Chahine M, Chen LQ, Barchi RL, Kallen RG, Horn R: Lidocaine block of human heart sodium channels expressed in xenopus oocytes. *J Mol Cell Cardiol* 1992; 24:1231-1236.
9. Roti Roti EC, Myers CD, Ayers RA, Boatman DE, Delfosse SA, Chan EK, Ackerman MJ, January CT, Robertson GA: Interaction with GM130 during HERG ion channel trafficking. Disruption by type 2 congenital long QT syndrome mutations. *Human Ether-a-go-go-Related Gene*. *J Biol Chem* 2002; 277:47779-47785.
10. Pasek M, Simurda J, Orchard CH, Christé G: A model of the guinea-pig ventricular cardiomyocyte incorporating a transverse-axial tubular system. *Prog Biophys Mol Biol* 2008; 96/1-3:258-280.
11. Zeng J, Laurita KR, Rosenbaum DS, Rudy Y, Laurita K, Rosenbaum D: Two components of the delayed rectifier K<sup>+</sup> current in ventricular myocytes of the guinea pig type. Theoretical formulation and their role in repolarization. *Circ Res* 1995; 77:140-152.

12. Wang S, Liu S, Morales MJ, Strauss HC, Rasmusson RL: A quantitative analysis of the activation and inactivation kinetics of HERG expressed in *Xenopus* oocytes. *J Physiol* 1997; 502:45-60.
13. Vandenberg JI, Varghese A, Lu Y, Bursill JA, Mahaut-Smith MP, Huang CL: Temperature dependence of human ether-a-go-go-related gene K<sup>+</sup> currents. *Am J Physiol* 2006; 291:C165-C175.
14. Millat G, Chevalier P, Restier-Miron L, Da Costa A, Bouvagnet P, Kugener B, Fayol L, Gonzalez AC, Oddou B, Chanavat V, Froidefond E, Perraudin R, Rousson R, Rodriguez-Lafrasse C: Spectrum of pathogenic mutations and associated polymorphisms in a cohort of 44 unrelated patients with long QT syndrome. *Clin Genet* 2006; 70:214-227.
15. Spector PS, Curran ME, Zou A, Keating MT, Sanguinetti MC: Fast inactivation causes rectification of the IKr channel. *J Gen Physiol* 1996; 107:611-619.
16. Sun Z, Milos PM, Thompson JF, Lloyd DB, Mank-Seymour A, Richmond J, Cordes JS, Zhou J: Role of a KCNH2 polymorphism (R1047L) in dofetilide-induced Torsades de Pointes. *J Mol Cell Cardiol* 2004; 37:1031-1039.
17. Zhou Z, Gong Q, Ye B, Fan Z, Makielski JC, Robertson GA, January CT: Properties of HERG channels stably expressed in HEK 293 cells studied at physiological temperature. *Biophys J* 1998; 74:230-241.
18. Priori S: Inherited arrhythmias database. Web page <http://www.fsm.it/cardmoc/2007>;
19. Gong Q, Keeney DR, Robinson JC, Zhou Z: Defective assembly and trafficking of mutant HERG channels with C-terminal truncations in long QT syndrome. *J Mol Cell Cardiol* 2004; 37:1225-1233.
20. Anderson CL, Delisle BP, Anson BD, Kilby JA, Will ML, Tester DJ, Gong Q, Zhou Z, Ackerman MJ, January CT: Most LQT2 mutations reduce Kv11.1 (hERG) current by a class 2 (trafficking-deficient) mechanism. *Circulation* 2006; 113:365-373.
21. Zhou Z, Gong Q, Epstein ML, January CT: HERG channel dysfunction in human long QT syndrome. Intracellular transport and functional defects. *J Biol Chem* 1998; 273:21061-21066.
22. Ficker E, Obejero-Paz CA, Zhao S, Brown AM: The binding site for channel blockers that rescue misprocessed human long QT syndrome type 2 ether-a-go-go-related gene (HERG) mutations. *J Biol Chem* 2002; 277:4989-4998.
23. Sanguinetti MC, Curran ME, Spector PS, Keating MT: Spectrum of HERG K<sup>+</sup>-channel dysfunction in an inherited cardiac arrhythmia. *Proc Natl Acad Sci U S A* 1996; 93:2208-2212.
24. Kagan A, Yu Z, Fishman GI, McDonald TV: The dominant negative LQT2 mutation A561V reduces wild-type HERG expression. *J Biol Chem* 2000; 275:11241-11248.
25. Aydar E, Palmer C: Functional characterization of the C-terminus of the human ether-a-go-go-related gene K(+) channel (HERG). *J Physiol* 2001; 534:1-14.

26. Choe CU, Schulze-Bahr E, Neu A, Xu J, Zhu ZI, Sauter K, Bähring R, Priori S, Guicheney P, Monnig G, Napolitano C, Heidemann J, Clancy CE, Pongs O, Isbrandt D: C-terminal HERG (LQT2) mutations disrupt IKr channel regulation through 14-3-3epsilon. *Hum Mol Genet* 2006; 15:2888-2902.
27. Sasano T, Ueda K, Orikabe M, Hirano Y, Kawano S, Yasunami M, Isobe M, Kimura A, Hiraoka M: Novel C-terminus frameshift mutation, 1122fs/147, of HERG in LQT2: additional amino acids generated by frameshift cause accelerated inactivation. *J Mol Cell Cardiol* 2004; 37:1205-1211.

## Legends to the table and figures

**Table 1:** Parameters (mean  $\pm$  sem) of COS7 cells transfected with either *WT* or mutated (hERG/A915fs+47X) plasmid. Numbers of cells is indicated in parentheses. \*\*\* denotes significant difference of mutant versus *WT* with  $P < 0.001$ .

**Figure 1: A:** Torsade de Pointes triggered by hypokalaemia in the proband. The horizontal bar represents 1 sec. **B:** Pedigree of the family (squares are males, circles females). The proband is marked with a + sign. Bearers of the mutations are in grey and are labelled 'del'. The family members that were tested and did not bear the mutation are labelled 'WT', numbers are the QTc values in ms.

**Figure 2:** Protein analysis. **A:** Typical Western blot produced on transfection of either 0.75 or 1.5  $\mu$ g cDNA (*WT* or *del* mut) in HEK293 cells. The *WT* hERG protein appears with the expected apparent molecular mass (160 kDa for the fully glycosylated form (fg) and 135 kDa for the core-glycosylated form (cg) of *WT*). *del* is considerably smaller at 120 (fg) and 100 kDa (cg) **B:** For 5 independent experiments, we computed the fg/cg ratio (fg image density) / (cg image density) for *WT* and for *del*. The bar diagram represents plots of the averaged fg/cg quotients (n=5) for both *WT* and *del* at the two different cDNA concentrations. The *del* quotients are significantly smaller (\* i.e.:  $p < 0.05$ , n=5) than *WT* quotients. **C:** Quantification of sucrose gradient analysis of *WT* and *del* proteins. The amount of protein recovered in each of the 24 fractions was quantified as image density on Western blots. Signals from an entire gradient were summed up and set at 100%. Average values of three independent experiments were plotted versus fraction numbers. Fractions 1 to 6 yielded no hERG protein and were not plotted. The analysis depicts two major peaks. The smaller peak to the left represents hERG

monomers and dimers, while the prominent peak to the right of the plot represents hERG tetramers.

**Figure 3:** Exploration of the current versus voltage relation in response to a two pulse protocol (insets to panels **A** and **B**): from a holding voltage at  $-80$  mV, a 2 s duration pulse P1 to a variable voltages between  $-80$  and  $+60$  mV in 10 mV increment was applied, followed by a 2 s test pulse P2 to  $-40$  mV. **A:** currents in a cell transfected with *WT*. A sum of two exponential functions plus offset was fitted to the current time course during each pulse (solid line). **B:** Representative example of currents recorded from a cell transfected with *del*.

**Figure 4:** Current-voltage relations in cells expressing hERG/*WT* (*WT*), hERG/A915fs+47X (*del*) or non transfected (NoH), the symbols and lines given in the inset of panel A apply to panels B, C and D. The voltage protocol is shown in figure 1 (inset). The numbers of cells and symbol definitions in panel A apply to panels B and C. **A:** Current measured at the end of the first pulse of the protocol versus pulse voltage. **B:** Maximal current during second pulse plotted versus voltage of first pulse. **C:** The average values of the peak tail current after background current subtraction and normalization are superimposed for *WT* and *del* to the steady-state activation variable ( $f_{act}$ ) versus voltage relations computed using a Boltzmann function and data in table 1. The two lines on the left are the inactivation versus voltage relations reconstructed for *WT* (dashed line) and for *del* (solid line) from data in table 1. **D:** Time constants of activation as evaluated using a 2-exponential fit to current traces from 75 ms to end of first pulse (figure 1). Symbols and lines are as defined in A. Dubious fitting results were eliminated and the size of the useful dataset is indicated near to each data point on the graph. **E:** Average peak tail currents in *Xenopus* oocytes injected with: buffer (open

triangles); 5 ng *WT* cDNA alone (filled circles); 5 ng *del* cDNA (open circles); 2.5 ng *WT* cDNA + 2.5 ng *del* cDNA (filled triangles). The voltage clamp protocol was the same as for COS7 cells.

**Figure 5:** Time constants of inactivation, as evaluated by fitting a single exponential function to the first 150 ms of the current at the beginning of pulse P3 (not shown, see protocol (3) in methods). Mean  $\pm$  sem for *WT* (squares) and for *del* (circles) are plotted versus voltage during P3. The number near each symbol is the number of cells. \*\*\* denotes significant difference of the two means with  $P < 0.001$  (Pearson's t-test).

**Figure 6:** Analysis of deactivation kinetics. **A:** Example of current responses to the protocol (inset) used for evaluating deactivation kinetics. Both the full size response to the second pulse and an expanded view of its initial region are shown. **B:** Time constant of recovery from inactivation versus voltage. **C:** Fast (hollow symbols) and slow (filled symbols) time constants of deactivation for *WT* (squares) and *del* (circles), plotted along a logarithmic vertical axis, versus second pulse command voltage. **D:** Example for one cell of the voltage dependence of amplitudes of the fast (squares) and the slow (triangles) exponential components of deactivation and of the infinity value of the current (circles), as resulted from the fits. The thick solid line is their sum and is also the fully activated I/V relation at time zero of pulse P2. **E, F and G** show the voltage dependence of the three components of current for *WT* (filled symbols) and *del* (hollow symbols). The data came from 13 cells expressing *WT* and 12 cells expressing *del*. Statistical significance of differences are reported as star signs: \*  $p < 0.05$ ; \*\*  $p < 0.01$ ; \*\*\*  $p < 0.001$ . **E:** The fraction of current decaying fast. **F:** The fraction of current decaying slowly. **G:** The fraction of non-decaying current.

**Figure 7:** Action potentials (APs) generated by the ventricular cell model. **A:** the duration of APs at 90% repolarization ( $APD_{90}$  as plotted as horizontal bars with exact values in ms at the right) were measured in the following situations. **(1):** At steady-state (after 100 beats) at 1 Hz with *WT*  $I_{Kr}$ . **(2 to 5):** From the steady-state action potential in case 1, various changes were applied and the  $APD_{90}$  of the next AP was measured. The changes were: **(2):** two-fold faster inactivation **(3):** altered deactivation pattern; **(4):** two-fold faster inactivation plus altered deactivation pattern; **(5):** halved  $I_{Kr}$  conductance only; **(6):** halved  $I_{Kr}$  conductance plus two-fold faster inactivation; **(7):** halved  $I_{Kr}$  conductance plus altered deactivation pattern; **(8):** all of the *del* mutation-induced changes. **B** and **C** respectively show action potential and  $I_{Kr}$  waveforms at steady-state either in *WT* (black lines) or after application of all mutation-related changes (*del*, grey lines).

		HERG/WT	HERG/A915fs+47X
$C_m$ (pF)		$44.6 \pm 3.0$ (53)	$41.8 \pm 1.8$ (49)
Maximal HERG tail current density (pA/pF)		$21.64 \pm 3.24$ (53)	$7.83 \pm 1.17$ (49)***
Steady state activation	$V_{ha}$ (mV)	$-0.2 \pm 1.2$ (53)	$1.9 \pm 1.8$ (49)
	$k_a$ (mV)	$-8.3 \pm 0.4$ (53)	$-8.6 \pm 0.6$ (49)
Steady state inactivation	$V_{hi}$ (mV)	$-62.9 \pm 5.7$ (7)	$-67.4 \pm 1.9$ (8)
	$k_i$ (mV)	$24.4 \pm 1.4$ (7)	$22.8 \pm 1.4$ (8)
$E_{rev}$ from instantaneous I/V		$-76.5 \pm 0.9$ (11)	$-77.4 \pm 0.4$ (18)

Table 1

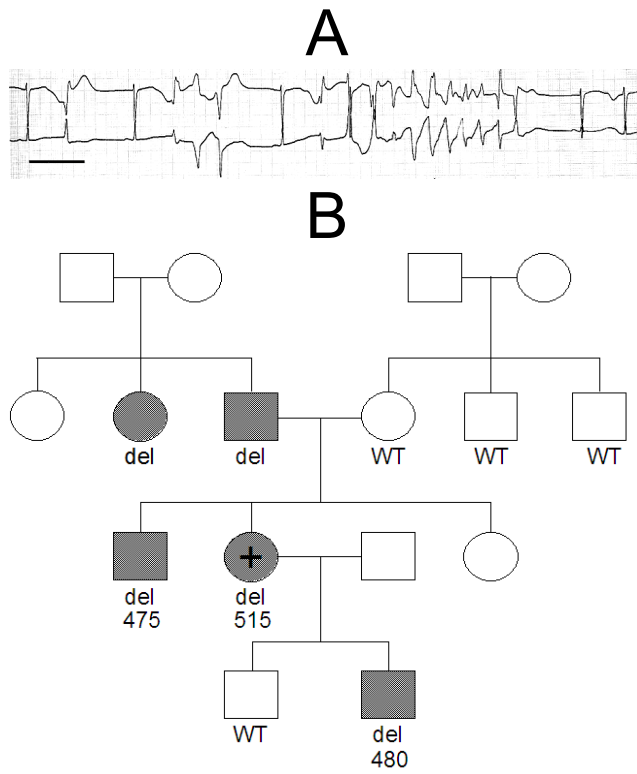


Figure 1

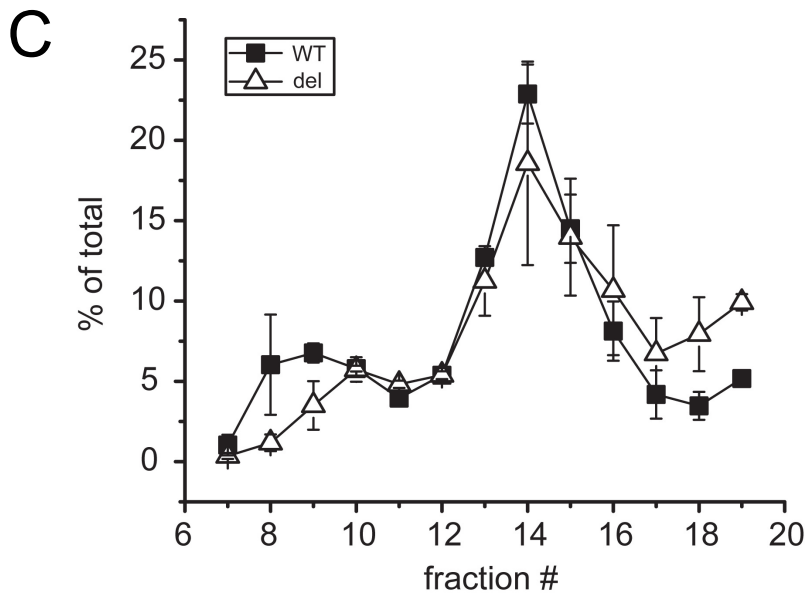
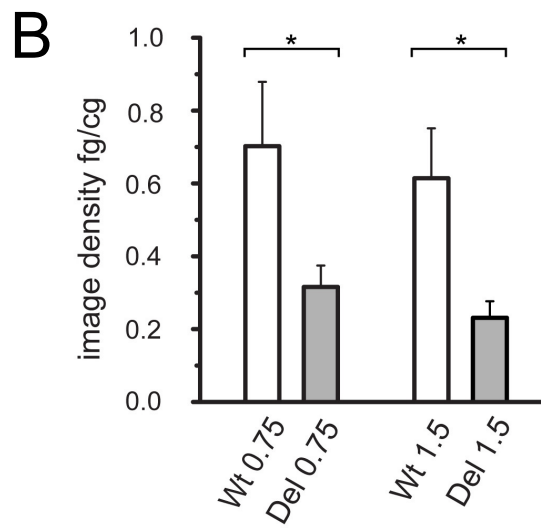
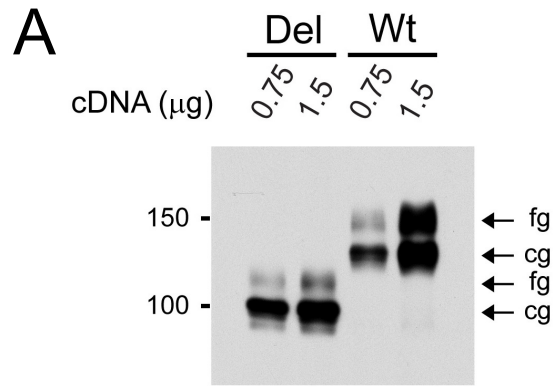


Figure 2

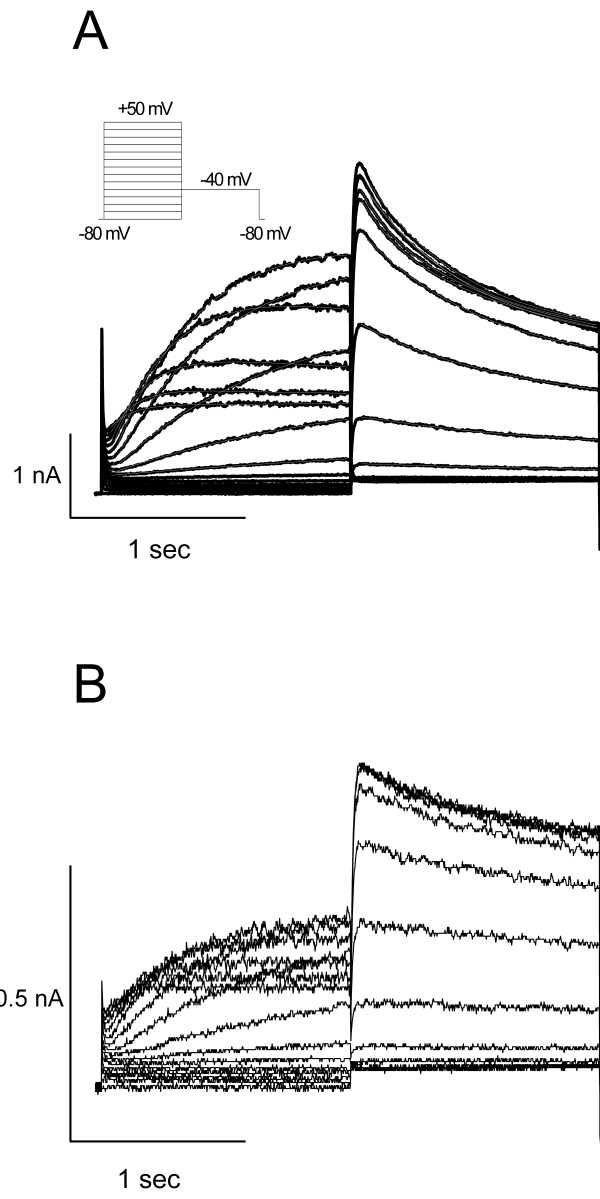


Figure 3

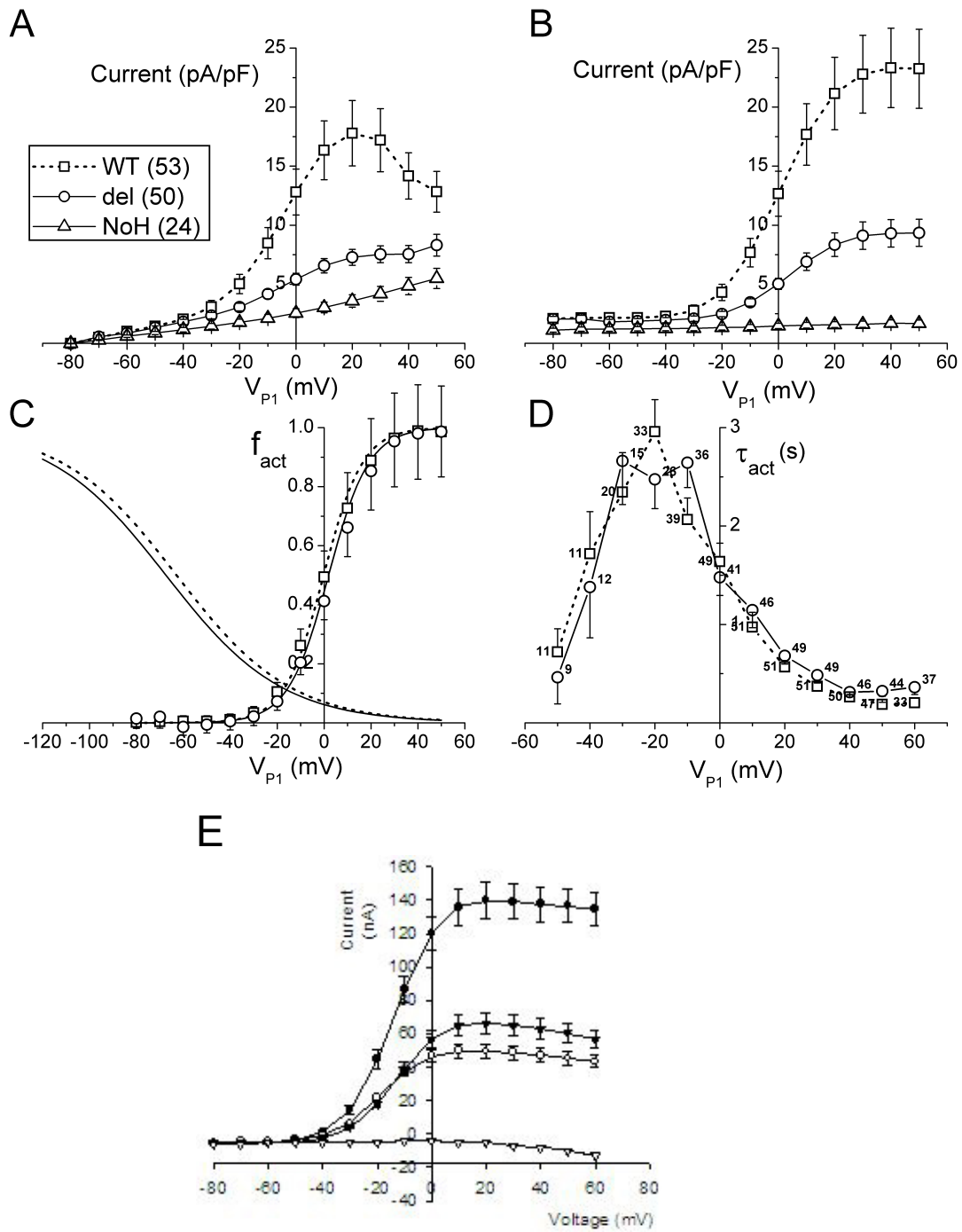


Figure 4

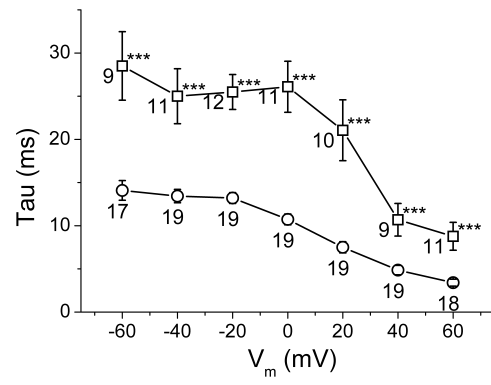


Figure 5

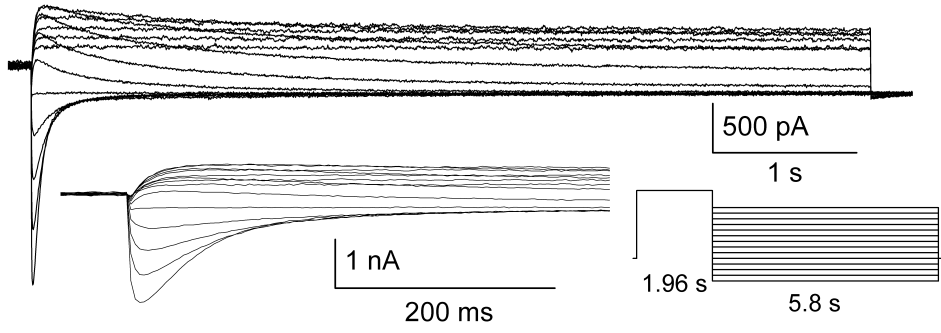
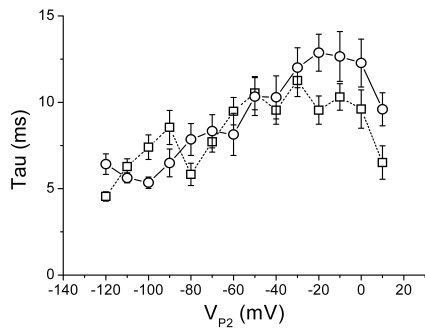
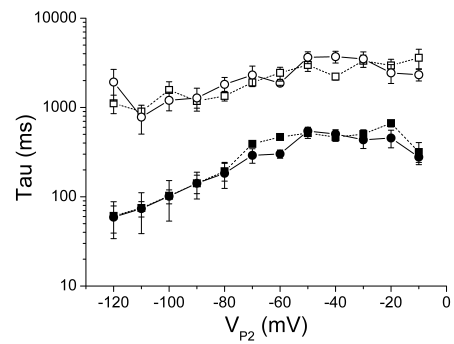
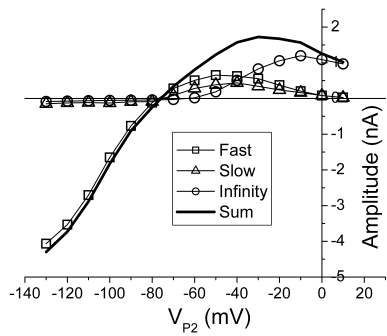
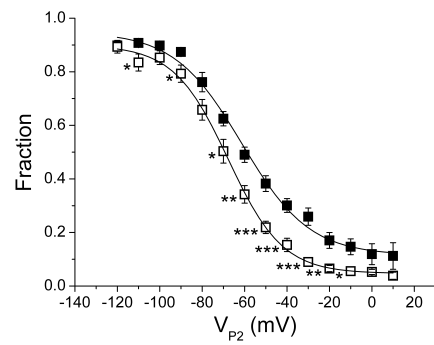
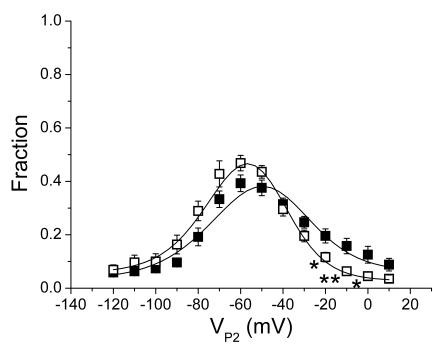
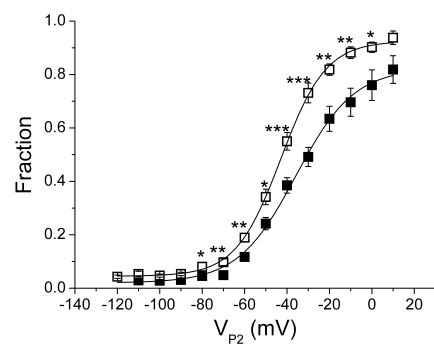
**A****B****C****D****E****F****G**

Figure 6

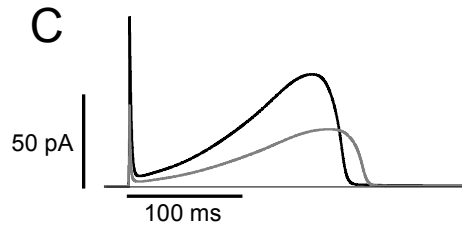
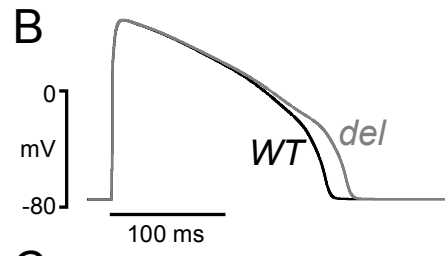
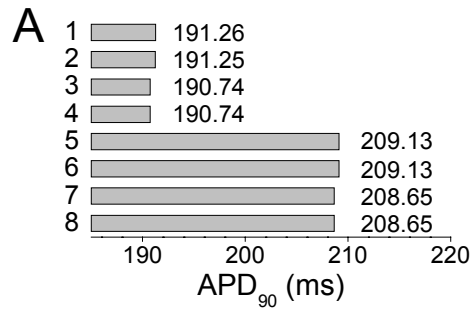


Figure 7